The mycobacterial cell wall partitions the plasma membrane to organize its own synthesis

Alam García-Heredia[1], Takehiro Kado[2], Caralyn E. Sein[2], Julia Puffal[2†], Sarah H. Osman[2], Julius Judd[3††], Todd A. Gray[3,4], Yasu S. Morita[1,2,*], M. Sloan Siegrist[1,2,*].

[1] Molecular and Cellular Biology Graduate Program, University of Massachusetts, Amherst, MA 01003, USA.

[2] Department of Microbiology, University of Massachusetts, Amherst, MA 01003, USA.

[3] Division of Genetics, Wadsworth Center, New York State Department of Health, Albany, NY 12208, USA.

[4] Department of Biomedical Sciences, University at Albany, Albany, NY 12208, USA.

[†] Present address: Department of Biochemistry and Molecular Biology, Rutgers University, Robert Wood Johnson Medical School, Piscataway, NJ 08854, USA.

[††] Present address: Department of Molecular Biology and Genetics, Cornell University, Ithaca, NY 14853, USA.

[*] Corresponding author. Email: siegrist@umass.edu (M.S.S.); ymorita@microbio.umass.edu (Y.S.M.).

Abstract

Many antibiotics target the assembly of cell wall peptidoglycan, an essential, heteropolymeric mesh that encases most bacteria. Different species have characteristic subcellular sites of peptidoglycan synthesis that they must carefully maintain for surface integrity and, ultimately, viability. In rod-shaped bacteria, cell wall elongation is spatially precise yet relies on a limited pool of lipid-linked precursors that generate and are attracted to membrane disorder. By tracking enzymes, substrates and products of peptidoglycan biosynthesis in *Mycobacterium smegmatis*, we show that precursors are made in plasma membrane domains that are laterally and biochemically distinct from sites of cell wall assembly. Membrane partitioning is required for robust, orderly peptidoglycan synthesis, indicating that these domains help template peptidoglycan synthesis. The cell wall-organizing protein DivIVA and the cell wall itself are essential for domain homeostasis. Thus, the peptidoglycan polymer feeds back on its membrane template to maintain an environment conducive to directional synthesis. We further show that our findings are applicable to rod-shaped bacteria that are phylogenetically distant from *M. smegmatis*, demonstrating that horizontal compartmentalization of precursors is a general feature of bacillary cell wall biogenesis.

40 **Main**

41 The final lipid-linked precursor for peptidoglycan synthesis, lipid II, is made by the
42 glycosyltransferase MurG in the inner leaflet of the plasma membrane. Lipid II is then flipped to
43 the outer leaflet by MurJ where its disaccharide-pentapeptide cargo is inserted into the existing
44 cell wall by membrane-bound transglycosylases and transpeptidases (Zhao et al., 2017). Early *in*
45 *vitro* work in *Staphylococcus aureus* and *Escherichia coli* indicated that a fluid
46 microenvironment might stimulate the activities of MurG and the upstream, lipid I synthase
47 MraY (Norris & Manners, 1993). More recent *in vivo* data has localized *Bacillus subtilis* MurG
48 to **r**egions of **i**ncreased **f**luidity (**RIF**s, [Muller et al., 2016; Strahl et al., 2014]), one of three
49 classes of membrane domains that have been described in bacteria to date. In mycobacteria,
50 **i**ntracellular **m**embrane **d**omains (IMD, formerly called PMf, [Morita et al., 2005]) can be
51 separated from the conventional plasma membrane (PM-CW, for **p**lasma **m**embrane associated
52 with **c**ell **w**all) by sucrose density gradient fractionation. The proteome and lipidome of IMD are
53 distinct from those of the PM-CW (Hayashi et al., 2016; Morita et al., 2005). Reanalysis of our
54 proteomics data (Hayashi et al., 2016) suggested that *Mycobacterium smegmatis* MurG is
55 enriched in the IMD while sequentially-acting transglycosylases and transpeptidases associate
56 with the PM-CW. While PM-CW-resident proteins distribute thorough the perimeter of live
57 mycobacteria, IMD-resident proteins localize along the sidewall but are enriched toward sites of
58 polar cell elongation (Hayashi et al., 2016; Hayashi et al., 2018). We also noted that polar
59 enrichment of MurG resembles that of the validated IMD marker GlfT2 (Hayashi et al., 2016;
60 Meniche et al., 2014), but that nascent peptidoglycan at the mycobacterial poles primarily abuts
61 rather than colocalizes with GlfT2 (Hayashi et al., 2018). These observations suggested a model
62 where lipid II synthesis is segregated from subsequent steps of cell wall assembly (Fig. 1A).

63

64 To test this model, we first expressed a functional MurG-Dendra2 fusion in *M. smegmatis*
65 (Figure 1–figure supplement 1A) and assayed its distribution in membrane fractions that had
66 been separated by density gradient (Fig. 1B). MurG-Dendra2, a peripheral membrane protein,
67 was enriched in both the cytoplasmic and IMD membrane fractions (Fig. 1C, top; Figure 1 –
68 figure supplement 2A). In intact cells, polar enrichment of MurG-Dendra2 was coincident with
69 that of the IMD marker mCherry-GlfT2 (Figure 2–figure supplement 1). This spatial relationship
70 was similar to that previously observed for MurG and GlfT2 (Hayashi et al., 2016; Hayashi et al.,
71 2018; Meniche et al., 2014).

72

73 Enzymes from the **p**enicillin **b**inding **p**roteins (PBPs) and **s**hape, **e**longation, **d**ivision and
74 **s**porulation (SEDS) families integrate the disaccharide-pentapeptide from lipid II into
75 peptidoglycan (Zhao et al., 2017). While our proteomics did not detect many polytopic
76 membrane proteins, including SEDS proteins, our PM-CW dataset was enriched for all known
77 PBPs (Hayashi et al., 2016). Fluorescent derivatives of β-lactam antibiotics, such as Bocillin-FL,
78 bind to PBPs and report transpeptidase-active enzymes. We incubated subcellular fractions from
79 wild-type *M. smegmatis* with Bocillin-FL and identified fluorescent proteins in the PM-CW (Fig.
80 1C, bottom; Figure 1 –figure supplement 2B). As expected for PBPs, the signal from these bands
81 was diminished by pre-treatment with ampicillin (Figure 1–figure supplement 3). We focused on
82 characterizing PonA1, an essential bifunctional transglycosylase/transpeptidase in *M. smegmatis*
83 (Hett et al., 2010; Kieser et al., 2015). Depletion of PonA1 (Hett et al., 2010) resulted in the loss
84 of the higher molecular band (Figure 1–figure supplement 3), confirming this protein is present

85 and active in the PM-CW (Fig. 1C, bottom). We next expressed a functional PonA1-mRFP
86 fusion in *M. smegmatis* (Kieser et al., 2015) and found that it was distributed around the cell
87 perimeter in a manner similar to the functional PM-CW marker PimE-GFP (Figure 1–figure
88 supplement 1B; Figure 2–figure supplement 1, [Hayashi et al., 2016]). Coexpression of MurG-
89 Dendra2 and PonA1-mRFP confirmed that the proteins are laterally segregated from one another
90 (Fig 2A). Together, our data show that MurG and PonA1 occupy membrane compartments that
91 are biochemically and spatially distinct.
92
93 The association of MurG with the IMD and of PonA1 with the PM-CW implied that the IMD is
94 the site of lipid II synthesis while the PM-CW is where peptidoglycan assembly takes place. We
95 refined an *in vitro* D-amino acid exchange assay to detect lipid-linked peptidoglycan precursors
96 from membrane fractions (Fig. 2B, [García-Heredia et al., 2018; Qiao et al., 2014]). In wild-type
97 cells, we detected biotinylated molecules in both the IMD and PM-CW (Fig. 2C; Figure 1–figure
98 supplement 2B). We hypothesized that the labeled species comprise precursors in both the inner
99 and outer leaflet of the plasma membrane. We and others have shown that depletion of MurJ
100 results in accumulation of biotinylated precursors (García-Heredia et al., 2018; Qiao et al., 2017).
101 By performing the D-amino acid exchange reaction on membrane fractions obtained from MurJ-
102 depleted *M. smegmatis* (Figure 1–figure supplement 1C), we found that precursors accumulate in
103 the IMD (Fig. 2C; Figure 1–figure supplement 2C). These results suggest that lipid II is made in
104 the IMD and transferred to the PM-CW in a MurJ-dependent manner.
105
106 Based on our biochemical data, we hypothesized that lipid II incorporation into the cell wall is
107 laterally segregated from its synthesis. We previously showed that alkynyl and azido D-amino

108 acid dipeptides (Liechti et al., 2014) incorporate into lipid-linked peptidoglycan precursors in *M.*
109 *smegmatis* (García-Heredia et al., 2018) and that metabolic labeling with alkynyl dipeptide
110 (alkDADA or EDA-DA, [Liechti et al., 2014]) is most intense in regions adjacent to the IMD
111 marker mCherry-GlfT2 (Hayashi et al., 2018). We labeled MurG-Dendra2-expressing *M.*
112 *smegmatis* with alkDADA and detected the presence of the alkyne by copper-catalyzed azide-
113 alkyne cycloaddition (CuAAC, [García-Heredia et al., 2018]). To distinguish extracellular
114 alkynes present in periplasmic lipid II and newly-polymerized cell wall from alkynes originating
115 from cytoplasmic lipid II, we selected picolyl azide-Cy3 as our label because of its poor
116 membrane permeability (Fig. 2B, [Yang & Hinner, 2015]). Using this optimized protocol, we
117 observed nascent peptidoglycan deposition at the polar tip, whereas MurG-Dendra2 was
118 proximal to this site (Fig. 2D). Our data suggest that lipid II synthesis is laterally partitioned
119 from the subsequent steps of peptidoglycan assembly. MurJ depletion reduced and delocalized
120 alkDADA-derived fluorescence (Figure 2–figure supplement 2), consistent with a gatekeeper
121 role for the flippase in both lateral membrane compartmentalization and flipping across the inner
122 membrane.
123
124 We next wanted to understand the effect of partitioning on cell wall synthesis. We opted to
125 perturb the plasma membrane with benzyl alcohol, which has been used to disperse membrane
126 domains in animal and bacterial cells, including *B. subtilis* RIFs (Muller et al., 2016; Nagy et al.,
127 2007). In *M. smegmatis,* we found that benzyl alcohol reduced the cellular material associated
128 with the IMD (Fig 3A, Figure 1–figure supplement 2D) and altered the distribution of FM4-64, a
129 non-specific lipophilic dye (Figure 3–figure supplement 1A) and of plasma membrane
130 glycolipids (Figure 3–figure supplement 2). However, benzyl alcohol did not alter labeling by N-

131 AlkTMM or O-AlkTMM (Figure 3–figure supplement 1B), probes that respectively mark the
132 noncovalent and covalent lipids of the outer 'myco' membrane (Foley et al., 2016). These
133 observations suggest that benzyl alcohol primarily affects the plasma membrane. MurG-Dendra2
134 was also notably less enriched in the IMD fraction following benzyl alcohol treatment (Fig. 1C,
135 top; Figure 1–figure supplement 2E) and, in live cells, at the poles (Fig. 2A). By contrast, benzyl
136 alcohol produced subtle changes in the subcellular distribution of active PBPs (Fig. 1C, bottom;
137 Figure 1–figure supplement 2D), although PonA1 shifted toward the poles in live cells (Fig. 2A).
138 Disruption of plasma membrane architecture was accompanied by dampening and delocalization
139 of peptidoglycan assembly (Fig. 3B) as well as a reduction in lipid precursor synthesis (Fig. 3C)
140 and halt in polar elongation (Figure 3–figure supplement 1B). The effects of benzyl alcohol were
141 reversible, as indicated by colony forming units and prompt recovery of peptidoglycan synthesis
142 (Figure 3–figure supplement 3). Dibucaine, a membrane-fluidizing anesthetic (Papahadjopoulos
143 et al., 1975), also delocalized IMD-resident proteins (Figure 3–figure supplement 4) and reduced
144 peptidoglycan synthesis (Fig. 3B). These data suggest that membrane architecture is essential
145 feature of both peptidoglycan synthesis and cell growth in *M. smegmatis*.
146
147 Benzyl alcohol delocalized or dampened cell wall assembly in other rod-shaped bacteria with
148 divergent envelope composition and modes of growth (Fig. 3D-E). Peptidoglycan synthesis was
149 less affected by benzyl alcohol in coccoid species, which lack MreB, and in rounded, A22-
150 treated *E. coli,* which have MreB inhibited (Fig. 3E). Thus, membrane partitioning is necessary
151 for effective, directional cell wall synthesis in rod-shaped bacteria.
152

153 How is the IMD partitioned away from the rest of the plasma membrane? The architecture of
154 eukaryotic membranes is influenced by transient links, or pinning, to the cytoskeleton (Fujimoto
155 & Parmryd, 2016; Liu et al., 2015). In *B. subtilis* and *E. coli,* actin homologs like MreB organize
156 RIFs (Oswald et al., 2016; Strahl et al., 2014) and direct peptidoglycan synthesis along the lateral
157 cell surface (Daniel & Errington, 2003; Iwai et al., 2002; Shi et al., 2018; Zhao et al., 2017).
158 While MreB is absent in mycobacteria, the essential tropomyosin-like protein DivIVA
159 concentrates cell wall assembly at the poles (Daniel & Errington, 2003; Iwai et al., 2002; Melzer
160 et al., 2018; Shi et al., 2018; Zhao et al., 2017). DivIVA depletion results in deformation and
161 rounding of mycobacterial cells (Kang et al., 2008). Given the similarities in DivIVA and MreB
162 function, we hypothesized that DivIVA creates and/or maintains the IMD. We used *M.*
163 *smegmatis* expressing DivIVA-eGFP-ID (in which DivIVA is fused to both eGFP and an
164 inducible degradation tag [Meniche et al., 2014]) to deplete DivIVA. Depletion of the protein
165 reduced the amount of IMD-associated cellular material (Fig. 4A, Figure 1–figure supplement
166 2F-G), altered the distribution of plasma membrane glycolipids (Figure 3–figure supplement 2),
167 and delocalized the IMD marker mCherry-GlfT2 from the poles (Fig. 4B). DivIVA
168 phosphorylation regulates MraY and/or MurG activity via an indirect, unknown mechanism (Jani
169 et al., 2010). Consistent with these data, we found that depletion of the protein reduced lipid-
170 linked peptidoglycan precursor abundance (Fig. 3C). The suppressive effects of benzyl alcohol
171 and DivIVA depletion on precursor abundance were not additive (Fig. 3C), suggesting that the
172 perturbations act on the same pathway.
173
174 As lipid II both generates and homes to disordered regions of model membranes (Ganchev et al.,
175 2006; Jia et al., 2011; Valtersson et al., 1985), the effect of DivIVA on precursors suggests that

176 concentrated peptidoglycan synthesis is a cause or a consequence (or both) of IMD/PM-CW
177 partitioning. In other organisms, lipid II production is required for MreB rotation (Dominguez-
178 Escobar et al., 2011; Garner et al., 2011; van Teeffelen et al., 2011) and to recruit MreB to the
179 plasma membrane (Schirner et al., 2015), so the precursor might also play an indirect role in
180 compartmentalizing the mycobacterial membrane via its influence on DivIVA. However, we
181 previously found that the IMD is biochemically intact after 8 hours of treatment with D-
182 cycloserine (Hayashi et al., 2018), an antibiotic that we have shown to block *M. smegmatis*
183 peptidoglycan precursor synthesis within 1 hour (García-Heredia et al., 2018). IMD-resident
184 proteins delocalize, but not until 6 hours of treatment. The persistence of IMD-resident proteins
185 and the time frame of delocalization indicate that concentrated lipid II synthesis is more likely a
186 consequence, rather than a cause, of mycobacterial membrane compartmentalization.
187
188 Our data supported a model in which DivIVA is necessary to maintain membrane partitioning,
189 which in turn supports efficient synthesis of peptidoglycan precursors and their precise
190 incorporation into the cell wall. However, we noted that eukaryotic membrane architecture can
191 also be influenced by transient interactions with external structures like extracellular matrix and
192 cellulose (Fujimoto & Parmryd, 2016; Liu et al., 2015). Furthermore, biophysical modeling of
193 bacteria suggests that osmotic pinning of the plasma membrane against the cell wall can induce
194 microphase separation (Mukhopadhyay et al., 2008). In mycobacteria, co-fractionation of the
195 **p**lasma **m**embrane and **c**ell **w**all (*i.e.* PM-CW) upon mechanical cell lysis implies that they are
196 physically connected (Morita et al., 2005). We wondered whether the peptidoglycan polymer
197 itself might contribute to the membrane partitioning that organizes its synthesis. To test this
198 hypothesis, we spheroplasted (enzymatically removed the cell wall; Melzer et al., 2018) *M.*

199 *smegmatis* that expressed MurG-Dendra2 or DivIVA-eGFP-ID and mCherry-GlfT2. All fusions
200 were functional (Figure 1–figure supplement 1, [Hayashi et al., 2016; Meniche et al., 2014]).
201 Fractionated lysates from spheroplasted mycobacteria had more diffuse distribution of cellular
202 material and indistinct separation of the IMD and PM-CW fractions (Fig. 4A). Consistent with
203 the macroscopic appearance of the fractionated lysate, MurG-Dendra2 was distributed
204 throughout the gradient (Figure 4–figure supplement 1). MurG-Dendra2 and the IMD marker
205 mCherry-GlfT2 were also diffusely distributed around the periphery of spheroplasted cells while
206 DivIVA, a non-IMD protein, remained in foci (Fig. 4C-D). These experiments indicate that an
207 intact cell wall and DivIVA are both required for membrane compartmentalization in *M.*
208 *smegmatis* (Fig. 4E).

209

210 While peptidoglycan biogenesis is well known to vertically span the inner and outer leaflets of
211 the plasma membrane, here we demonstrate in *M. smegmatis* that it is also horizontally
212 partitioned. Partitioning of the mycobacterial membrane by DivIVA and the cell wall follows
213 similar logic to that of eukaryotic membranes, which can be compartmentalized by pinning to
214 cytoplasmic structures such as the actin cytoskeleton and to external structures like extracellular
215 matrix and cellulose (Fujimoto & Parmryd, 2016; Liu et al., 2015), and of model lipid bilayers,
216 which can be phase separated by adhesive forces (Gordon et al., 2008; Mukhopadhyay et al.,
217 2008). In mycobacteria, however, the membrane regions that promote cell wall synthesis are
218 segregated by the end product of the pathway (Fig. 4E). For these and other rod-shaped bacteria,
219 our model is that the membrane-cell wall axis is a self-organizing system in which directed cell
220 wall synthesis organizes the plasma membrane, and an organized plasma membrane in turn
221 makes cell wall elongation more efficient and precise.

Acknowledgments

We are grateful to Drs. James Chambers and Amy Burnside for microscopy and flow cytometry guidance, Drs. Eric Strieter and Jiaan Liu and Ms. Sylvia Rivera and Katherine Chacón-Vargas for technical assistance. We also thank Drs. Hesper Rego and Eric Rubin for *ponA1-mRFP M. smegmatis,* Dr. Christopher Sassetti for the MurJ and MurG depletion strains, and Dr. Benjamin Swarts for O-AlkTMM and N-AlkTMM. Research was supported by funds from the National Institutes of Health (NIH) under awards R21 AI144748 (Y.S.M and M.S.S.), U01 CA221230 and NIH DP2 AI138238 (M.S.S.) and R03 AI140259-01 (Y.S.M.), and R01 AI097191 (J.J. and T.A.G.). A.G.-H. was supported by an Honors Fellowship from Universidad Autónoma de Nuevo León. J.P. is a recipient of the Science Without Boarders Fellowship from CAPES-Brazil (0328-13-8). T.K. was supported by a postdoctoral fellowship from Uehara Memorial Foundation.

Contributions

M.S.S., A.G.-H. and Y.S.M. designed the experiments and analyzed the data. A.G.-H. performed most of the experiments. T.K. constructed the DivIVA-eGFP-ID/mCherry-GlfT2 *M. smegmatis* mutant and helped with experiments from Figs. 3B, 4B and Figure 3–figure supplement 4. J.P. performed immunoblots for Figure 1–figure supplement 2 and thin-layer chromatography for Figure 3–figure supplement 2. C.E.S performed experiments for Fig. 4C.

S.H.O. did experiments for Fig. 4A and Figure 4–figure supplement 1. Y.S.M. did the glycolipid analysis for Figure 1–figure supplement 1. J.J. and T.A.G. constructed the MurG-Dendra2 plasmid. M.S.S. and A.G.-H. wrote the manuscript. All authors reviewed and edited the manuscript.

Competing interests

Authors declare no competing interests.

Data and materials availability

All data are available in the main text or the supplementary materials. Raw data is available at open science framework through the next link:
https://osf.io/fm794/?view_only=7d5a24b82dd94744a46420aee09bad7f

Figure supplements

Supplementary information: Tables S1-4

References

Daniel, R. A., & Errington, J. (2003). Control of cell morphogenesis in bacteria: two distinct ways to make a rod-shaped cell. *Cell, 113*(6), 767-776. doi:10.1016/s0092-8674(03)00421-5

Dominguez-Escobar, J., Chastanet, A., Crevenna, A. H., Fromion, V., Wedlich-Soldner, R., & Carballido-Lopez, R. (2011). Processive movement of MreB-associated cell wall

biosynthetic complexes in bacteria. *Science, 333*(6039), 225-228. doi:10.1126/science.1203466

Foley, H. N., Stewart, J. A., Kavunja, H. W., Rundell, S. R., & Swarts, B. M. (2016). Bioorthogonal Chemical Reporters for Selective In Situ Probing of Mycomembrane Components in Mycobacteria. *Angew Chem Int Ed Engl, 55*(6), 2053-2057. doi:10.1002/anie.201509216

Fujimoto, T., & Parmryd, I. (2016). Interleaflet Coupling, Pinning, and Leaflet Asymmetry-Major Players in Plasma Membrane Nanodomain Formation. *Front Cell Dev Biol, 4*, 155. doi:10.3389/fcell.2016.00155

Ganchev, D. N., Hasper, H. E., Breukink, E., & de Kruijff, B. (2006). Size and orientation of the lipid II headgroup as revealed by AFM imaging. *Biochemistry, 45*(19), 6195-6202. doi:10.1021/bi051913e

García-Heredia, A., Pohane, A. A., Melzer, E. S., Carr, C. R., Fiolek, T. J., Rundell, S. R., . . . Siegrist, M. S. (2018). Peptidoglycan precursor synthesis along the sidewall of pole-growing mycobacteria. *Elife, 7*. doi:10.7554/eLife.37243

Garner, E. C., Bernard, R., Wang, W., Zhuang, X., Rudner, D. Z., & Mitchison, T. (2011). Coupled, circumferential motions of the cell wall synthesis machinery and MreB filaments in B. subtilis. *Science, 333*(6039), 222-225. doi:10.1126/science.1203285

Gee, C. L., Papavinasasundaram, K. G., Blair, S. R., Baer, C. E., Falick, A. M., King, D. S., . . . Alber, T. (2012). A phosphorylated pseudokinase complex controls cell wall synthesis in mycobacteria. *Sci Signal, 5*(208), ra7. doi:10.1126/scisignal.2002525

Gordon, V. D., Deserno, M., Andrew, C. M. J., Egelhaaf, S. U., & Poon, W. C. K. (2008). Adhesion promotes phase separation in mixed-lipid membranes. *EPL (Europhysics Letters), 84*(4), 48003. doi:10.1209/0295-5075/84/48003

Hayashi, J. M., Luo, C. Y., Mayfield, J. A., Hsu, T., Fukuda, T., Walfield, A. L., . . . Morita, Y. S. (2016). Spatially distinct and metabolically active membrane domain in mycobacteria. *Proc Natl Acad Sci U S A, 113*(19), 5400-5405. doi:10.1073/pnas.1525165113

Hayashi, J. M., Richardson, K., Melzer, E. S., Sandler, S. J., Aldridge, B. B., Siegrist, M. S., & Morita, Y. S. (2018). Stress-Induced Reorganization of the Mycobacterial Membrane Domain. *MBio, 9*(1). doi:10.1128/mBio.01823-17

Hett, E. C., Chao, M. C., & Rubin, E. J. (2010). Interaction and modulation of two antagonistic cell wall enzymes of mycobacteria. *PLoS Pathog, 6*(7), e1001020. doi:10.1371/journal.ppat.1001020

Iwai, N., Nagai, K., & Wachi, M. (2002). Novel S-benzylisothiourea compound that induces spherical cells in Escherichia coli probably by acting on a rod-shape-determining protein(s) other than penicillin-binding protein 2. *Biosci Biotechnol Biochem, 66*(12), 2658-2662. doi:10.1271/bbb.66.2658

Jani, C., Eoh, H., Lee, J. J., Hamasha, K., Sahana, M. B., Han, J. S., . . . Kang, C. M. (2010). Regulation of polar peptidoglycan biosynthesis by Wag31 phosphorylation in mycobacteria. *BMC Microbiol, 10*, 327. doi:10.1186/1471-2180-10-327

Jia, Z., O'Mara, M. L., Zuegg, J., Cooper, M. A., & Mark, A. E. (2011). The effect of environment on the recognition and binding of vancomycin to native and resistant forms of lipid II. *Biophys J, 101*(11), 2684-2692. doi:10.1016/j.bpj.2011.10.047

Kang, C. M., Nyayapathy, S., Lee, J. Y., Suh, J. W., & Husson, R. N. (2008). Wag31, a homologue of the cell division protein DivIVA, regulates growth, morphology and polar

cell wall synthesis in mycobacteria. *Microbiology, 154*(Pt 3), 725-735. doi:10.1099/mic.0.2007/014076-0

Kieser, K. J., Boutte, C. C., Kester, J. C., Baer, C. E., Barczak, A. K., Meniche, X., . . . Rubin, E. J. (2015). Phosphorylation of the Peptidoglycan Synthase PonA1 Governs the Rate of Polar Elongation in Mycobacteria. *PLoS Pathog, 11*(6), e1005010. doi:10.1371/journal.ppat.1005010

Kumar, S., Stecher, G., Li, M., Knyaz, C., & Tamura, K. (2018). MEGA X: Molecular Evolutionary Genetics Analysis across Computing Platforms. *Mol Biol Evol, 35*(6), 1547-1549. doi:10.1093/molbev/msy096

Liechti, G. W., Kuru, E., Hall, E., Kalinda, A., Brun, Y. V., VanNieuwenhze, M., & Maurelli, A. T. (2014). A new metabolic cell-wall labelling method reveals peptidoglycan in Chlamydia trachomatis. *Nature, 506*(7489), 507-510. doi:10.1038/nature12892

Liu, Z., Persson, S., & Sanchez-Rodriguez, C. (2015). At the border: the plasma membrane-cell wall continuum. *J Exp Bot, 66*(6), 1553-1563. doi:10.1093/jxb/erv019

Melzer, E. S., Sein, C. E., Chambers, J. J., & Sloan Siegrist, M. (2018). DivIVA concentrates mycobacterial cell envelope assembly for initiation and stabilization of polar growth. *Cytoskeleton (Hoboken), 75*(12), 498-507. doi:10.1002/cm.21490

Meniche, X., Otten, R., Siegrist, M. S., Baer, C. E., Murphy, K. C., Bertozzi, C. R., & Sassetti, C. M. (2014). Subpolar addition of new cell wall is directed by DivIVA in mycobacteria. *Proc Natl Acad Sci U S A, 111*(31), E3243-3251. doi:10.1073/pnas.1402158111

Morita, Y. S., Sena, C. B., Waller, R. F., Kurokawa, K., Sernee, M. F., Nakatani, F., . . . Maeda, Y. (2006). PimE is a polyprenol-phosphate-mannose-dependent mannosyltransferase that transfers the fifth mannose of phosphatidylinositol mannoside in mycobacteria. *Journal of Biological Chemistry*.

Morita, Y. S., Velasquez, R., Taig, E., Waller, R. F., Patterson, J. H., Tull, D., . . . McConville, M. J. (2005). Compartmentalization of lipid biosynthesis in mycobacteria. *J Biol Chem, 280*(22), 21645-21652. doi:10.1074/jbc.M414181200

Mukhopadhyay, R., Huang, K. C., & Wingreen, N. S. (2008). Lipid localization in bacterial cells through curvature-mediated microphase separation. *Biophys J, 95*(3), 1034-1049. doi:10.1529/biophysj.107.126920

Muller, A., Wenzel, M., Strahl, H., Grein, F., Saaki, T. N. V., Kohl, B., . . . Hamoen, L. W. (2016). Daptomycin inhibits cell envelope synthesis by interfering with fluid membrane microdomains. *Proc Natl Acad Sci U S A, 113*(45), E7077-e7086. doi:10.1073/pnas.1611173113

Nagy, E., Balogi, Z., Gombos, I., Akerfelt, M., Bjorkbom, A., Balogh, G., . . . Vigh, L. (2007). Hyperfluidization-coupled membrane microdomain reorganization is linked to activation of the heat shock response in a murine melanoma cell line. *Proc Natl Acad Sci U S A, 104*(19), 7945-7950. doi:10.1073/pnas.0702557104

Norris, V., & Manners, B. (1993). Deformations in the cytoplasmic membrane of Escherichia coli direct the synthesis of peptidoglycan. The hernia model. *Biophys J, 64*(6), 1691-1700. doi:10.1016/S0006-3495(93)81541-8

Oswald, F., Varadarajan, A., Lill, H., Peterman, E. J., & Bollen, Y. J. (2016). MreB-Dependent Organization of the E. coli Cytoplasmic Membrane Controls Membrane Protein Diffusion. *Biophys J, 110*(5), 1139-1149. doi:10.1016/j.bpj.2016.01.010

Paintdakhi, A., Parry, B., Campos, M., Irnov, I., Elf, J., Surovtsev, I., & Jacobs-Wagner, C. (2016). Oufti: an integrated software package for high-accuracy, high-throughput

quantitative microscopy analysis. *Mol Microbiol, 99*(4), 767-777. doi:10.1111/mmi.13264

Papahadjopoulos, D., Jacobson, K., Poste, G., & Shepherd, G. (1975). Effects of local anesthetics on membrane properties. I. Changes in the fluidity of phospholipid bilayers. *Biochim Biophys Acta, 394*(4), 504-519. doi:10.1016/0005-2736(75)90137-6

Qiao, Y., Lebar, M. D., Schirner, K., Schaefer, K., Tsukamoto, H., Kahne, D., & Walker, S. (2014). Detection of lipid-linked peptidoglycan precursors by exploiting an unexpected transpeptidase reaction. *J Am Chem Soc, 136*(42), 14678-14681. doi:10.1021/ja508147s

Qiao, Y., Srisuknimit, V., Rubino, F., Schaefer, K., Ruiz, N., Walker, S., & Kahne, D. (2017). Lipid II overproduction allows direct assay of transpeptidase inhibition by beta-lactams. *Nat Chem Biol, 13*(7), 793-798. doi:10.1038/nchembio.2388

Schindelin, J., Arganda-Carreras, I., Frise, E., Kaynig, V., Longair, M., Pietzsch, T., . . . Cardona, A. (2012). Fiji: an open-source platform for biological-image analysis. *Nat Methods, 9*(7), 676-682. doi:10.1038/nmeth.2019

Schirner, K., Eun, Y. J., Dion, M., Luo, Y., Helmann, J. D., Garner, E. C., & Walker, S. (2015). Lipid-linked cell wall precursors regulate membrane association of bacterial actin MreB. *Nat Chem Biol, 11*(1), 38-45. doi:10.1038/nchembio.1689

Sena, C. B., Fukuda, T., Miyanagi, K., Matsumoto, S., Kobayashi, K., Murakami, Y., . . . Morita, Y. S. (2010). Controlled expression of branch-forming mannosyltransferase is critical for mycobacterial lipoarabinomannan biosynthesis. *Journal of Biological Chemistry*, jbc. M109. 077297.

Shi, H., Bratton, B. P., Gitai, Z., & Huang, K. C. (2018). How to Build a Bacterial Cell: MreB as the Foreman of E. coli Construction. *Cell, 172*(6), 1294-1305. doi:10.1016/j.cell.2018.02.050

Strahl, H., Burmann, F., & Hamoen, L. W. (2014). The actin homologue MreB organizes the bacterial cell membrane. *Nat Commun, 5*, 3442. doi:10.1038/ncomms4442

Valtersson, C., van Duyn, G., Verkleij, A. J., Chojnacki, T., de Kruijff, B., & Dallner, G. (1985). The influence of dolichol, dolichol esters, and dolichyl phosphate on phospholipid polymorphism and fluidity in model membranes. *J Biol Chem, 260*(5), 2742-2751. Retrieved from https://www.ncbi.nlm.nih.gov/pubmed/3919007

van Teeffelen, S., Wang, S., Furchtgott, L., Huang, K. C., Wingreen, N. S., Shaevitz, J. W., & Gitai, Z. (2011). The bacterial actin MreB rotates, and rotation depends on cell-wall assembly. *Proc Natl Acad Sci U S A, 108*(38), 15822-15827. doi:10.1073/pnas.1108999108

Yang, N. J., & Hinner, M. J. (2015). Getting across the cell membrane: an overview for small molecules, peptides, and proteins. *Methods Mol Biol, 1266*, 29-53. doi:10.1007/978-1-4939-2272-7_3

Zhao, H., Patel, V., Helmann, J. D., & Dorr, T. (2017). Don't let sleeping dogmas lie: new views of peptidoglycan synthesis and its regulation. *Mol Microbiol, 106*(6), 847-860. doi:10.1111/mmi.13853

Main figures

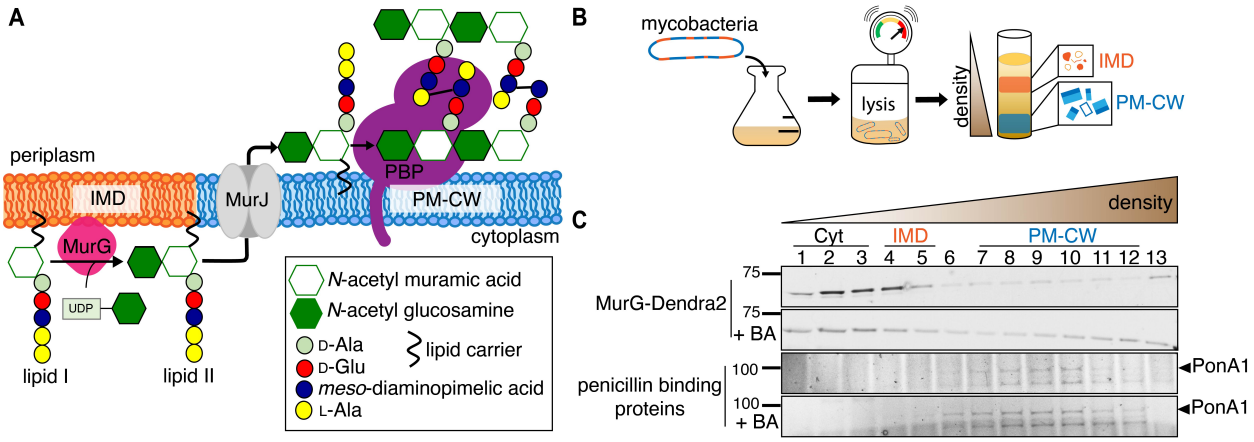

Fig. 1. MurG is enriched in the IMD and PBPs associate with PM-CW. (A) Membrane-bound steps of peptidoglycan synthesis with hypothesized partitioning into IMD and PM-CW. (B) Bacteria are lysed by nitrogen cavitation and cell lysate is sedimented on a sucrose density gradient. (C) Lysates from wild-type or MurG-Dendra2-expressing *M. smegmatis* were fractionated as in (B) and separated by SDS-PAGE. Top, in-gel fluorescence shows MurG-Dendra2 association with the IMD. Treatment with benzyl alcohol (BA) redistributed the protein across the fractions. Bottom, wild-type *M. smegmatis* membrane fractions were incubated with Bocillin-FL prior to SDS-PAGE. Labeled PBPs are enriched in PM-CW.

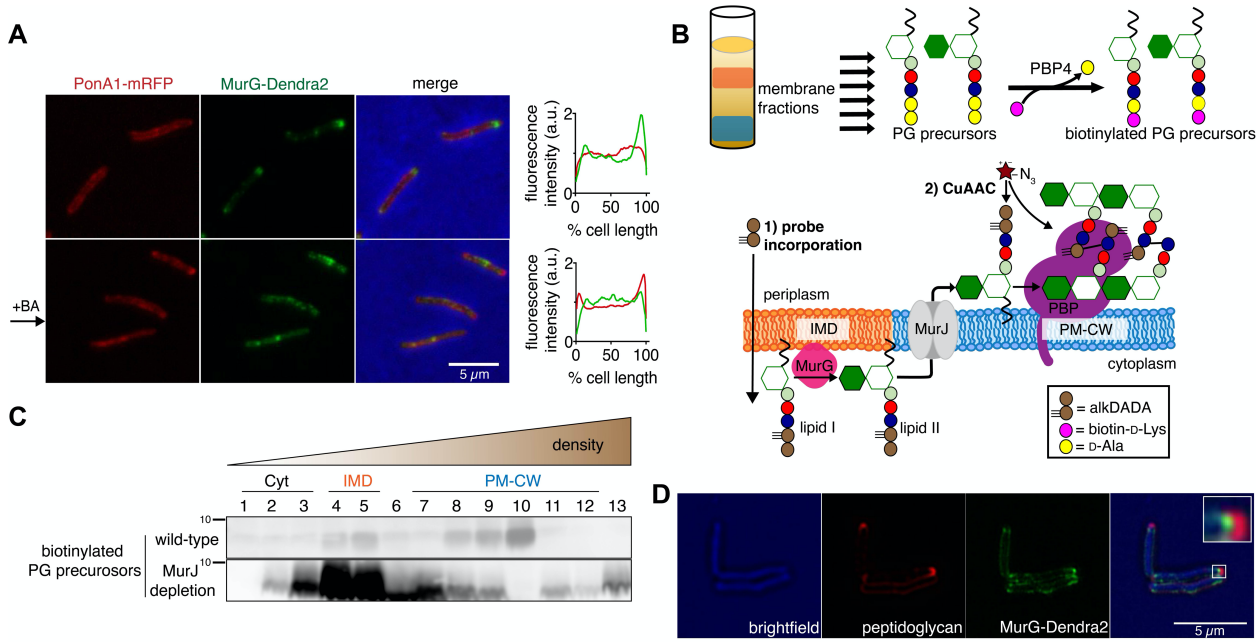

Fig. 2. Lipid II is synthesized in the IMD and trafficked to the PM-CW. (A) Left, conventional microscopy of *M. smegmatis* coexpressing PonA1-mRFP and MurG-Dendra2 treated +/- benzyl alcohol (BA). Right, fluorescence distribution of the fusion proteins. a.u., arbitrary units. (B) Top, detection scheme for lipid-linked peptidoglycan (PG) precursors from membrane fractions. Bottom, metabolic labeling scheme of mycobacterial cell wall synthesis (García-Heredia et al., 2018). (C) PG precursors are labeled as in (B), top. The labeled precursors are in the IMD and PM-CW of wild-type *M. smegmatis* but accumulate in the IMD upon MurJ depletion (García-Heredia et al., 2018). (D) *M. smegmatis* expressing MurG-Dendra2 were incubated with alkDADA. Surface-exposed alkynes on fixed cells were detected by CuAAC (García-Heredia et al., 2018). Cells imaged by structured illumination microscopy (SIM-E).

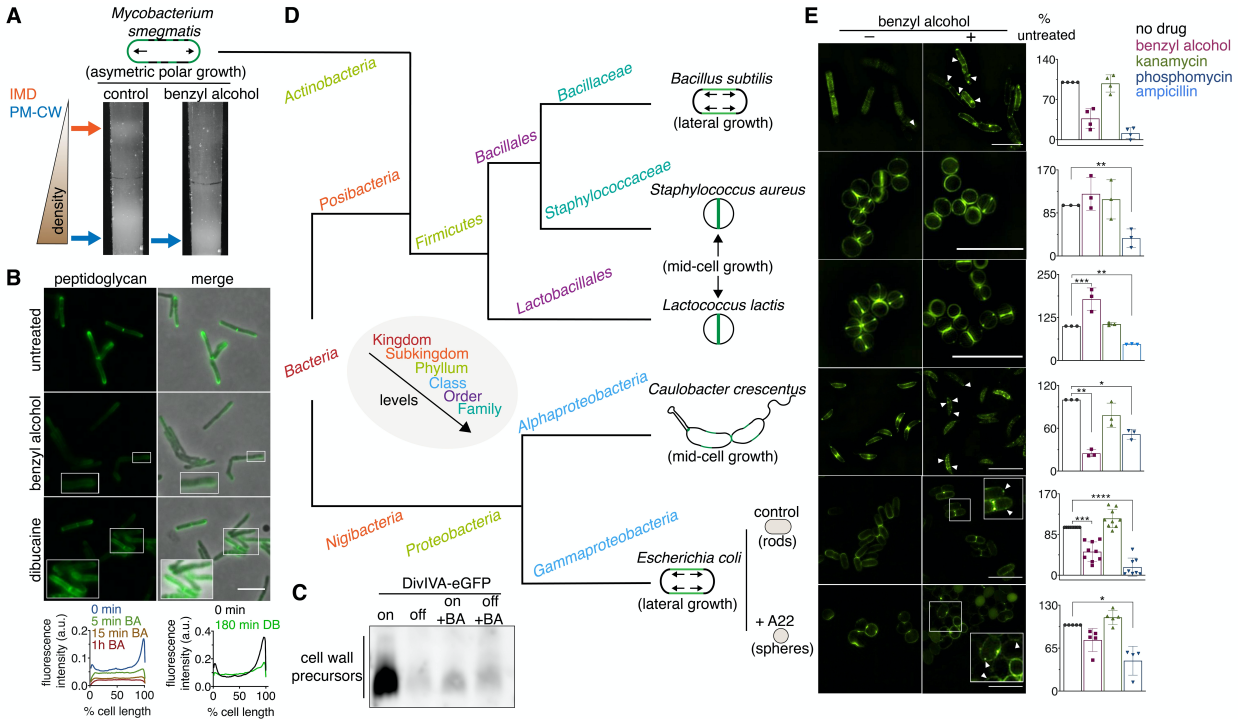

Fig. 3. Membrane perturbations disrupt peptidoglycan biogenesis in *M. smegmatis* and phylogenetically-distant bacilli. (A) Lysates from wild-type *M. smegmatis* treated +/- benzyl alcohol (BA) were sedimented in a sucrose density gradient. (B) Top, wild-type *M. smegmatis* was incubated or not with benzyl alcohol or dibucaine, then labeled with alkDADA. Bottom, the distribution of peptidoglycan labeling from wild-type *M. smegmatis* that was incubated with BA or dibucaine (DB) for the indicated time was quantitated as in Fig. 2A, except that signal intensity was not normalized. (C) DivIVA-eGFP-ID *M. smegmatis* was either treated with benzyl alcohol, depleted of DivIVA, or both, and the peptidoglycan precursors from whole cells were biotinylated as in Fig. 2B, top. (D) Phylogenetic tree constructed with 16S rDNA sequences (rate of mutation not considered). Taxonomic groups matched with colors to their levels with only diverging points shown. Shapes and growth modes illustrated for select species. (E) Left, different bacteria treated +/- benzyl alcohol followed by alkDADA incubation. Arrowheads highlight irregular patches of peptidoglycan. Insets are magnified. Where applicable, *E. coli* was preincubated with A22. Right, bacteria were treated with benzyl alcohol, translation-inhibiting kanamycin, or peptidoglycan-acting phosphomycin or ampicillin then labeled as in (B) and analyzed by flow cytometry (see Methods). Median fluorescence intensity (MFI) values were normalized to untreated controls and experiments were performed 3-9 times in triplicate. Error bars, +/- standard deviation of biological replicates. *, $p < 0.05$; **, $p < 0.005$; ***, $p < 0.0005$; ****, $p < 0.00005$, ratio paired t-tests and one-way ANOVA with Dunnet´s test for non-normalized MFI of biological replicates. Scale bars, 5 µm.

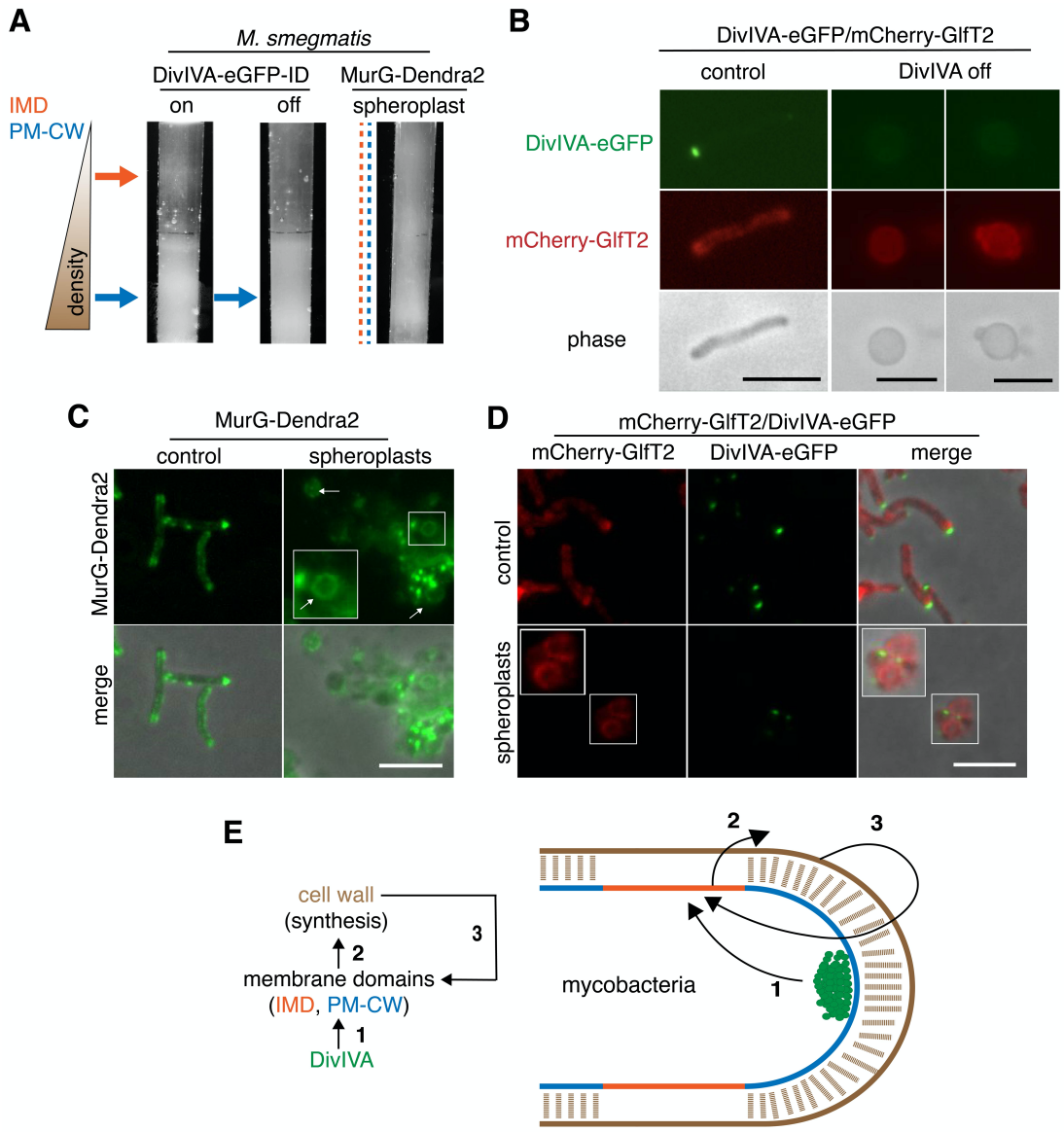

Fig. 4. Plasma membrane domains are maintained by DivIVA and the cell wall. (A) Lysates from MurG-Dendra2- or DivIVA-eGFP-ID-expressing *M. smegmatis* that had been depleted of DivIVA (Meniche et al., 2014) or spheroplasted (Melzer et al., 2018), were sedimented in a density gradient. (B). DivIVA was depleted or not in *M. smegmatis* expressing both DivIVA-eGFP-ID and mCherry-GlfT2. Normally, DivIVA localizes at the polar tip and mCherry-GlfT2 concentrates proximal to DivIVA. Depletion of DivIVA delocalizes mCherry-GlfT2. *M. smegmatis* expressing MurG-Dendra2 (C) or coexpressing mCherry-GlfT2 and DivIVA-eGFP-ID (D) were spheroplasted or not and imaged. In spheroplasted cells, the IMD-associated proteins distribute along the cell periphery. Arrows mark spheroplasts outside and within insets, which have increased size and brightness. (E) Model for self-organization of plasma membrane and cell wall in *M. smegmatis*. Brown line indicates the cell wall. Short brown lines perpendicular to the membrane and cell wall indicate that the cell wall is likely to be physically connected to the membrane in the PM-CW regions (Morita et al., 2005). All scale bars, 5 µm.

463 **Methods**

464 **Bacterial strains and growth conditions**

465 *Mycobacterium smegmatis* mc^{2}155 was grown in Middlebrook 7H9 growth medium (BD Difco,
466 Franklin Lakes, NJ USA) supplemented with 0.4% (v/v) glycerol, 0.05% (v/v) Tween-80
467 (Sigma-Aldrich, St. Louis, MO USA) and 10% ADC (albumin-dextrose-catalase) as well as
468 apramycin (50 µg/mL), kanamycin (25 µg/mL; Sigma-Aldrich, St. Louis, MO USA) and
469 hygromycin (50 µg/mL) where appropriate. *Staphylococcus aureus* ATCC BA-1718 was grown
470 in BHI (BD Difco, Franklyn Lakes NJ, USA); *Escherichia coli* K12 and *Bacillus subtilis* ZB307,
471 in LB (VWR, Radnor PA, USA); *Caulobacter crescentus* NA 1000, in peptone yeast extract (BD
472 Difco, Franklyn Lakes NJ, USA); and *Lactococcus lactis* NRRL B633, in MRS (Oxoid,
473 Basingstoke, Hampshire UK). All bacteria were grown shaking at 37ºC with the exception of *C.*
474 *crescentus*, which was incubated at 30ºC. See Table S3 for more information.

475

476 **Mutant strain construction**

477 To test the function of PimE-GFP-FLAG fusion, an expression vector for PimE-GFP-FLAG
478 (pYAB186) (Hayashi et al., 2016) was electroporated into a *pimE* deletion mutant (Morita et al.,
479 2006). Three independent colonies were picked for the phenotypic complementation of AcPIM6
480 biosynthetic defects. Lipid purification and analysis were performed as described previously
481 (Morita et al., 2006).

482

483 The *murG* gene was amplified by PCR from *M. smegmatis* mc^{2}155 genomic DNA by PCR,
484 excluding the stop codon, and was inserted into pMSR in-frame with mycobacterial codon-
485 optimized Dendra2 using In-Fusion cloning (Takara Bio, Mountain View, CA USA). This
486 construct was transformed by electroporation into *M. smegmatis* mc^{2}155, where it integrates at
487 the L5 *attB* site, and was selected by apramycin treatment. Constitutive expression of the MurG-
488 Dendra2 fusion was achieved through the Psmyc promoter (GenBank: AF395207.1). The
489 plasmid construct was validated by Sanger sequencing.

490

491 To replace the endogenous *glfT2* gene with a gene encoding HA-mCherry-GlfT2 in the DivIVA-
492 eGFP-ID strain, we electroporated pMUM052 (Hayashi et al., 2016) into DivIVA-eGFP-ID *M.*
493 *smegmatis*, and positive clones were isolated using hygromycin resistance marker and SacB-
494 dependent sucrose sensitivity. Correct replacement of the *glfT2* gene was confirmed by PCR.

495

496 **Generation of spheroplasts**

497 To generate spheroplasts, we followed a previous protocol (Melzer et al., 2018). Briefly, wild-
498 type, MurG-Dendra2-expressing or mCherry-GlfT2/DivIVA-eGFP-ID-coexpressing *M.*
499 *smegmatis* was grown until log phase. Glycine (1.2% w/v final concentration) was added and the
500 culture was incubated for 24 h at 37ºC with shaking. Afterwards, the cells were washed with
501 sucrose-$MgCl_2$-maleic acid (SMM) buffer (pH 6.8) and harvested by centrifugation (4000 x *g* for
502 5 min). The pellet was resuspended in 7H9 medium where the water was replaced with SMM
503 buffer; the medium also was supplemented with glycine (1.2% final concentration) and lysozyme

504 (50 µg/mL final concentration). Bacteria were incubated another 24 h at 37ºC with shaking, and
505 then spheroplasts where either imaged by conventional fluorescence microscopy or lysed by
506 nitrogen cavitation immediately for subsequent biochemical analysis.

507

508 **Membrane fractionation**

509 Log phase *M. smegmatis* (that, where applicable, were untreated, treated with benzyl alcohol,
510 depleted for DivIVA or spheroplasted; see Table S1) were harvested by centrifugation and
511 washed in PBS + 0.05% Tween-80 (PBST). One gram of wet pellet was resuspended in 5 mL of
512 lysis buffer containing 25 mM HEPES (pH 7.4), 20% (w/v) sucrose, 2 mM EGTA, and a
513 protease inhibitor cocktail (Thermo Fisher Scientific, Waltham, MA USA) as described (Morita
514 et al., 2005). Bacteria were lysed using nitrogen cavitation at 2000 psi for 30 min three times.
515 Cell lysates were centrifuged at 3220 x *g* for 10 min at 4ºC twice to remove unlysed cells prior to
516 loading on a 20-50% sucrose gradient. Membrane-containing fractions were collected in 1 mL
517 after ultracentrifugation at 35,000 rpm on an SW-40 rotor (Beckman, Brea, CA USA) for 6 hours
518 at 4ºC and stored at -80ºC prior to analysis.

519

520 **Detection of proteins in membrane fractions**

521 MurG-Dendra2 and penicillin-binding proteins (PBPs) were detected by in-gel fluorescence. For
522 MurG-Dendra2, membrane fractions were incubated with an equal volume of 2x loading buffer
523 and then separated by SDS-PAGE on a 12% polyacrylamide gel. To detect PBPs, 50 µg total

524 protein from wild-type *M. smegmatis* membrane fractions were incubated with 40 µM of
525 Bocillin-FL (Thermo Fisher Scientific, Waltham, MA USA) for 30 min in the dark at 37ºC. An
526 equal volume of 2x loading buffer was then added and the mixture was boiled for 3 min at 95ºC
527 and then incubated on ice for 30 min. Membrane mixtures were separated on a 12%
528 polyacrylamide gel. Gels were washed in distilled water and imaged using an ImageQuant LAS
529 4000mini (GE Healthcare, Chicago, IL USA).

530

531 MurJ, PimB´ and MptA were detected by immunoblot. Briefly, cell lysate or membrane fraction
532 proteins were separated by SDS-PAGE on a 12% polyacrylamide gel and transferred to a PVDF
533 membrane. The membrane was blocked with 3% milk in PBS + 0.05% Tween-80 (PBST) and
534 then incubated overnight with primary antibodies (monoclonal mouse anti-FLAG [to detect
535 MurJ; Sigma], and polyclonal rabbit anti-PimB´ or anti-MptA antibodies (Sena et al., 2010).
536 Antibodies were detected with appropriate secondary antibodies conjugated to horseradish
537 peroxidase (GE Healthcare, Chicago, Il USA). Membranes were rinsed in PBS + 0.05% Tween-
538 20 and visualized by ECL in an ImageQuant LAS 4000mini (GE Healthcare, Chicago, IL USA)
539 as above.

540

541 **Cell envelope labeling**

542 Chemical probes used in this work include alkDADA (Liechti et al., 2014), N-AlkTMM and O-
543 AlkTMM (Foley et al., 2016) and FM4-64 FX (Invitrogen, Carlsbad, CA USA). AlkDADA was
544 synthesized by the Einstein Chemical Biology Core and the TMM probes were kind gifts of Dr.

545 Ben Swarts. Unless otherwise indicated, mid-log *M. smegmatis* or, where applicable, *B. subtilis,*
546 *S. aureus, E. coli, L. lactis* or *C. crescentus* were labeled with 2 mM alkDADA, 250 μM N-
547 AlkTMM, 50 μM O-AlkTMM or 5 μg/mL FM4-64FX for 15 min or 5 min in the case of *B.*
548 *subtilis*. Unless otherwise indicated and where applicable, the bacteria were pre-incubated in the
549 presence or absence of freshly-prepared chemicals (antibiotics or benzyl alcohol) before being
550 subjected to the probes (see Table S1 and S2). Cells were pelleted by centrifugation, washed in
551 PBST containing 0.01% BSA (PBSTB) and fixed for 10 min in 2% formaldehyde at room
552 temperature. For alkDADA and O-AlkTMM, cells were further washed twice with PBSTB and
553 subjected to CuAAC as described (García-Heredia et al., 2018). Unless otherwise specified,
554 picolyl azide-Cy3 was used in Fig. 2D; picolyl azide carboxyrhodamine 110 was used in Figs.
555 3B, 3D and Figure 2–figure supplement 2, Figure 3–figure supplement 1, and Figure 3–figure
556 supplement 3. Bacteria were then washed twice in PBSTB, once in PBST, and imaged (described
557 below) or subjected to flow cytometry (BD DUAL LSRFortessa, UMass Amherst Flow
558 Cytometry Core).

559

560 **Microscopy and image analysis**

561 Bacteria were imaged on agar pads by either conventional fluorescence microscopy (Nikon
562 Eclipse E600, Nikon Eclipse Ti or Zeiss Axioscope A1 with 100x objectives) or structured
563 illumination microscopy (Nikon SIM-E/A1R with SR Apo TIRF 100x objective, UMass
564 Amherst Light Microscopy Core).

565 To obtain the fluorescence intensity plots, the subcellular distribution of fluorescence was
566 quantitated from images obtained by conventional fluorescence microscopy. The images were
567 processed using Fiji and Oufti (Paintdakhi et al., 2016; Schindelin et al., 2012) as described
568 (García-Heredia et al., 2018). The signal was normalized to length and total fluorescence
569 intensity of the cell. Cells were oriented such that the brighter pole is on the right-hand of the
570 graph. The intensity plots from Fig. 2A were made from 42<n<56 cells; for Fig. 3B, from
571 14<n<70 cells.

572

573 **Evaluation of membrane-bound peptidoglycan precursors**

574 Wild-type or MurJ-depleted *M. smegmatis* (Gee et al., 2012) were grown to mid-log phase and
575 membrane fractions were isolated as above. Precursors were extracted from each membrane
576 fraction similar to previous publications (García-Heredia et al., 2018; Qiao et al., 2014; Qiao et
577 al., 2017). Briefly, glacial acetic acid was added to 500 µL of fractionated lysate to a final
578 volume of 1%. The sample was then transferred into a vial containing 500 µL of chloroform and
579 1 mL of methanol and left at room temperature for 1-2 hours with occasional vortexing. The
580 mixture was centrifuged at 21,000x *g* for 10 min and the supernatant was transferred into a vial
581 containing 500 µL of 1% glacial acetic acid (in water) and 500 µL chloroform, and vortexed for
582 1 min. The mixture was separated by centrifugation (900x *g* for 1 min at room temperature) and
583 the organic phase was collected. Where applicable, the white interface was reextracted to recover
584 additional organic material. The organic phase was dried under a nitrogen stream and the dried
585 lipids were resuspended in 12 µL of DMSO. D-amino acid-containing, lipid-linked
586 peptidoglycan precursors were biotinylated by subjecting organic extracts to an *in vitro* PBP4-

587 mediated exchange reaction with biotin-D-lysine (Chem-Impex International, Wood Dale, IL
588 USA; reagent was deprotected first) as described (Qiao et al., 2014). The products were
589 separated by SDS-PAGE on an 18%, polyacrylamide gels then transferred to a PVDF membrane,
590 blotted with streptavidin-HRP (diluted 1:10,000; Thermo Fisher Scientific, Waltham, MA USA)
591 and visualized by ECL as above.

592

593 **Membrane glycolipid analysis**

594 Sucrose density gradient fractions from wild-type *M. smegmatis* +/- 1 hour of 100 mM benzyl
595 alcohol treatment or DivIVA-eGFP-ID with DivIVA depleted or not (Meniche et al., 2014) were
596 subjected to lipid purification and analysis as previously described (Morita et al., 2005).

597

598 **Phylogenetic analysis**

599 The phylogenetic tree was made in Adobe Illustrator (version 23.0.3) based on a phylogenetic
600 tree generated with Mega (version 7.0.26; Kumar et al., 2018). Briefly, 16S rDNA sequences
601 were obtained from NCBI (see Table S2) and aligned using ClustalW. The phylogenetic tree was
602 generated using the Timura-Ney model with Gamma distribution and Bootstrap method (1000
603 replications). The taxonomic information was verified with the Interagency Taxonomic
604 Information System (available online https://www.itis.gov/).

605

606 **Figure supplements**

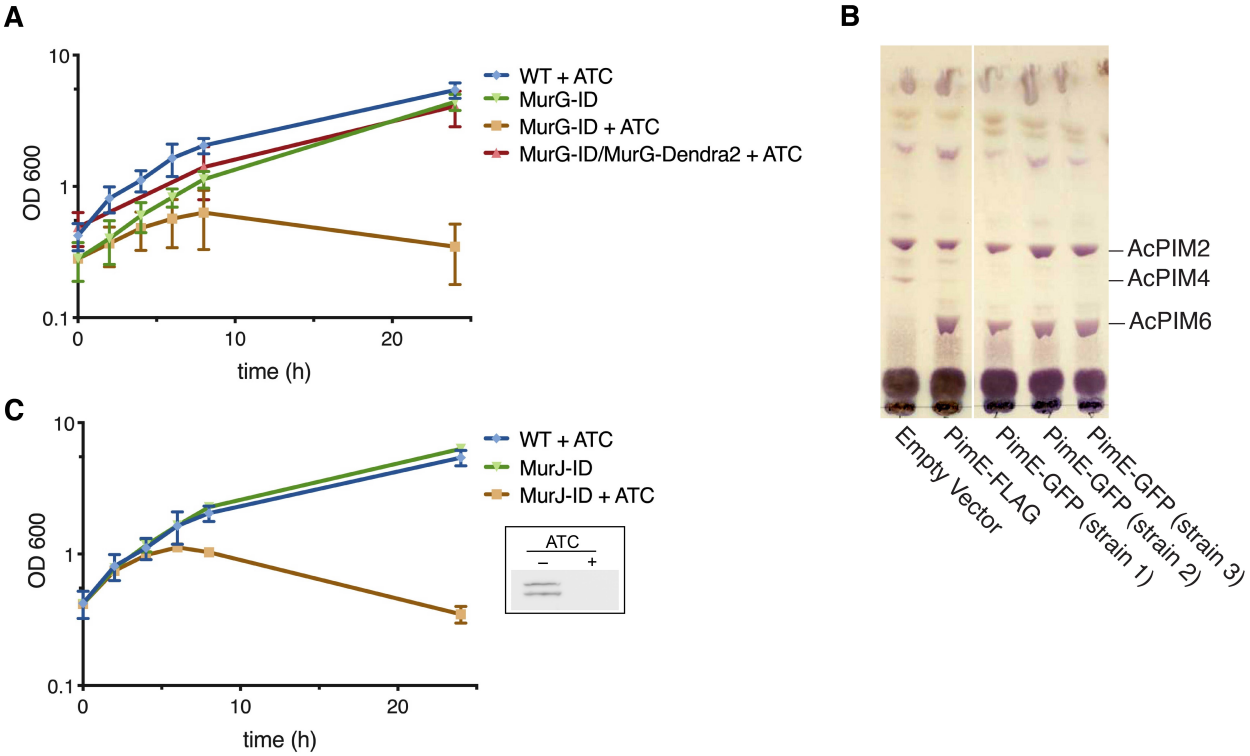

607

608 **Figure 1–figure supplement 1.** MurG-Dendra2 and PimE-GFP are functional, and MurJ can be
609 depleted. (A) MurG-Dendra2 expression rescues depletion of endogenous protein. MurG
610 depletion strain (Meniche et al., 2014) was transformed with a plasmid containing *murG-*
611 *dendra2* and grown +/- 50 ng/mL anhydrotetracycline (ATC) to induce MurG-ID degradation.
612 (B) PimE-GFP is functional. PimE is a mannosyltransferase involved in phosphatidylinositol
613 mannoside (PIM) biosynthesis, converting AcPIM4 to more polar PIMs. Δ*pimE* was
614 complemented with the indicated expression vectors. Glycolipids were extracted, purified, and
615 separated by thin-layer chromatography. PIMs were visualized by orcinol staining. Similar to
616 PimE-FLAG (Morita et al., 2006), PimE-GFP can restore the production of AcPIM6. (C) MurJ is
617 depleted upon treatment with anhydrotetracycline (ATC). Depletion strain (MurJ-ID; carrying
618 FLAG tag) was grown +/- ATC. Insert, immunoblot of lysates showing that MurJ is degraded
619 after 8 hours of ATC treatment as reported (Gee et al., 2012).

620

621

622

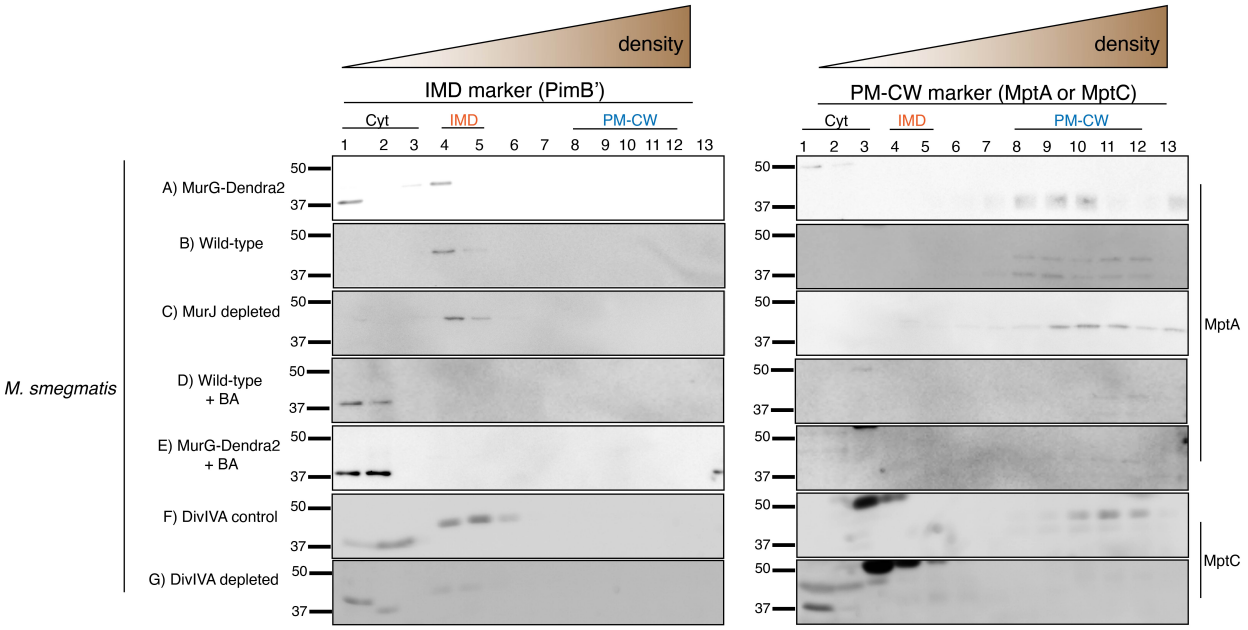

Figure 1 –figure supplement 2. Western blot analysis of the IMD and the PM-CW membrane fractions separated by sucrose density sedimentation. Antibodies against PimB' and MptA or MptC were used to detect the IMD and PM-CW, respectively (Hayashi et al., 2016; Sena et al., 2010). Analyzed fractions shown here are the same fractions of: A) MurG-Dendra2-expressing cells as shown in Fig. 1C; B) wild-type cells as shown in Fig. 1C and Fig. 2C; C) MurJ-depleted cells as shown in Fig. 2C; D) wild-type cells treated with benzyl alcohol (BA) as shown in Fig. 1C; E) MurG-Dendra2-expressing cells treated with benzyl alcohol as shown in Fig. 1C; F) and G) are DivIVA-eGFP-ID where DivIVA was depleted or not depleted as in Fig 4A. Samples from F) and G) were concentrated 10-fold by precipitating proteins in chloroform and water. PimB' appears as ~45 kDa band in the IMD fractions but disappears upon BA treatment or DivIVA depletion. We do not yet know the reason for this disappearance. The band at ~37 kDa, which is visible especially in the cytoplasmic fractions of BA-treated cells is a non-specific protein (Hayashi et al., 2016). MptA and MptC appear as ~42 kDa band in the PM-CW fractions, which became fainter after BA treatment or depletion of DivIVA.

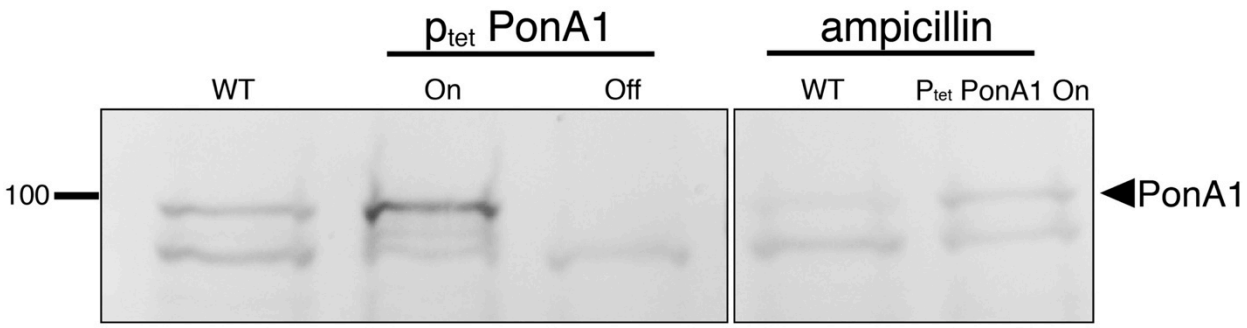

Figure 1–figure supplement 3. Visualization of PonA1 using Bocillin-FL. To assess specificity of the fluorescent signal, membrane fractions were pre-incubated +/- 16 µg/mL ampicillin and 5 µg/mL of the β-lactamase inhibitor clavulanate (García-Heredia et al., 2018) for 30 min at room temperature. 100 µg of total membrane proteins were incubated with 40 µM of Bocillin-FL for 30 min, then separated by SDS-PAGE (12% gel) and visualized by in-gel fluorescence to detect PBPs. WT, wild-type *M. smegmatis*; p_{tet}*ponA1* expressed (On) or depleted (Off) with addition of anhydrotetracycline (ATC) as described (Hett et al., 2010).

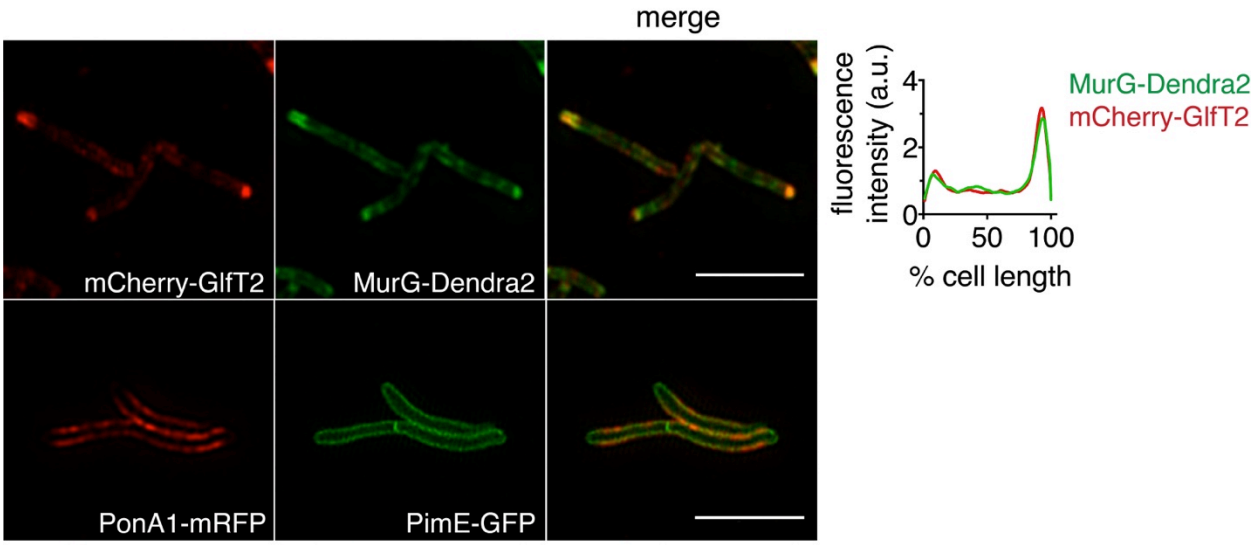

Figure 2–figure supplement 1. MurG-Dendra2 and PonA1-mRFP colocalize with IMD and PM-CW reporters, respectively. *M. smegmatis* coexpressing MurG-Dendra2 and mCherry-GlfT2 or PonA1-mRFP and PimE-GFP were imaged by SIM-E. Scale bars, 5 µm. Graph, the fluorescence intensity profiles of the proteins were quantitated as in Fig 2A from images captured with conventional microscopy.

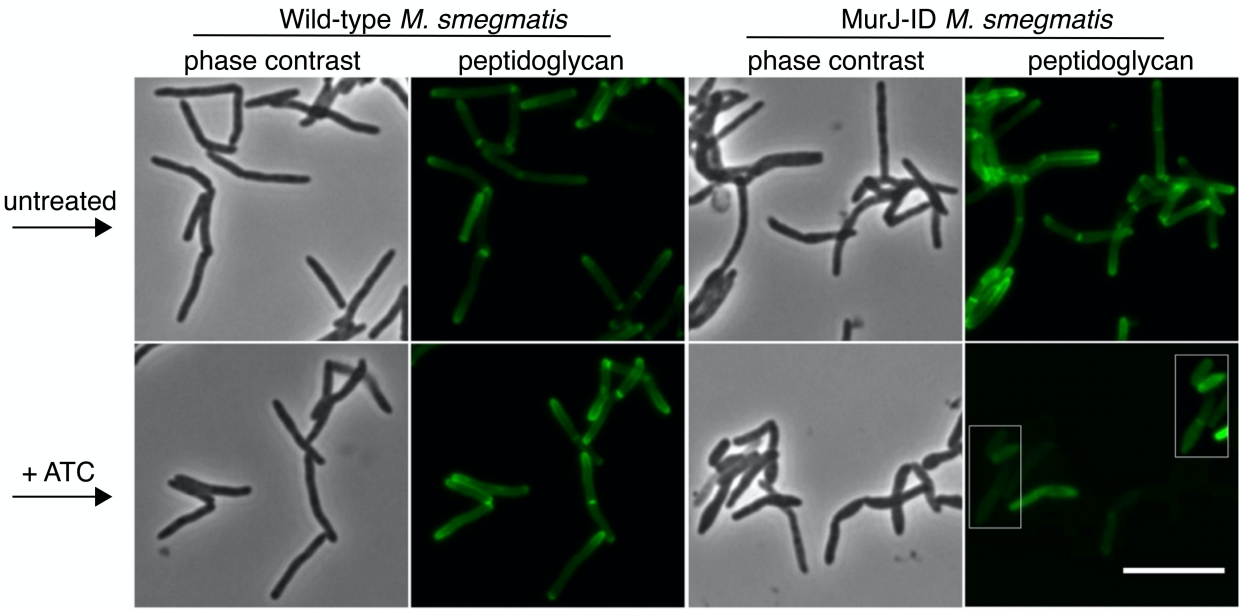

679

680 **Figure 2–figure supplement 2.** Depletion of MurJ alters amount and location of nascent
681 peptidoglycan. Wild-type (left) or MurJ-ID (depletion strain; right) *M. smegmatis* in early log
682 phase were treated +/ anhydrotetracycline (ATC) then incubated with alkDADA. Bacteria were
683 washed, fixed, subjected to CuAAC and imaged by conventional fluorescence microscopy. Scale
684 bar, 5 μm.

685

686

687

688

689

690

691

692

693

694

695

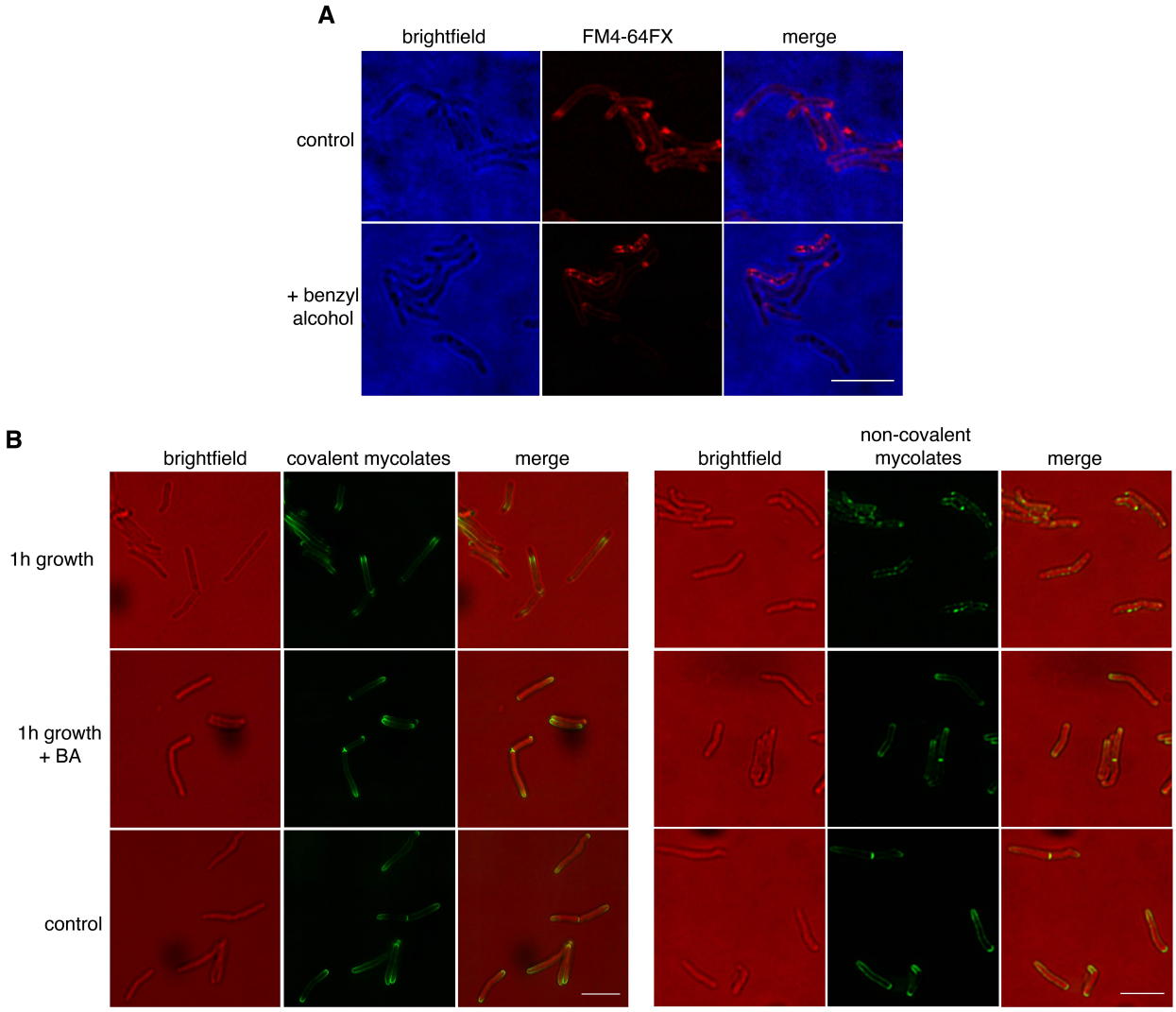

Figure 3–figure supplement 1. (A) Benzyl alcohol alters FM4-64FX distribution. Wild-type *M. smegmatis* was labeled with FM4-64FX, then washed and incubated with benzyl alcohol. Cells were then imaged with SIM-E. (B) Benzyl alcohol halts cell elongation but does not otherwise impact the localization of mycomembrane probes. Wild-type *M. smegmatis* was incubated with O-AlkTMM (left) or N-AlkTMM (right) to label covalent or noncovalent mycolates, respectively, then washed and subjected or not to benzyl alcohol for 1 hour. Bacteria were washed, fixed, subjected to CuAAC and imaged by conventional fluorescence microscopy. As a control, bacteria were not treated with benzyl alcohol for 1 hour, *i.e.* fixed immediately after probe incubation (bottom panel). All scale bars, 5 µm.

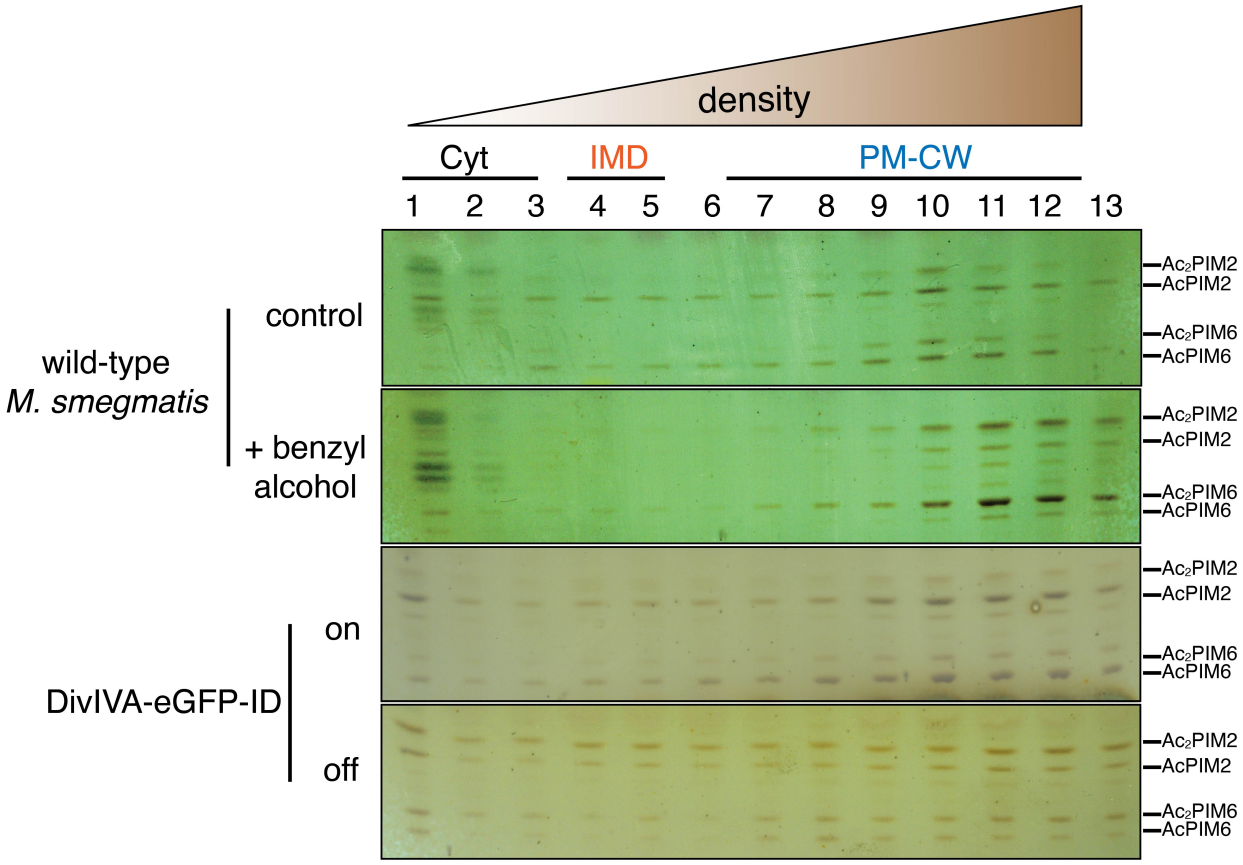

Figure 3–figure supplement 2. Benzyl alcohol and depletion of DivIVA affect the distribution of membrane glycolipids. Wild-type or DivIVA-eGFP-ID *M. smegmatis* were treated +/- benzyl alcohol or ATC, respectively. PIMs were visualized by orcinol staining as in Figure 1–figure supplement 1. AcPIM2 and AcPIM6 present during normal growth in the IMD and are diminished upon benzyl alcohol treatment. Depletion of DivIVA is accompanied by an enrichment of PIM2 species and depletion of PIM6 species. This change in lipids is currently under investigation.

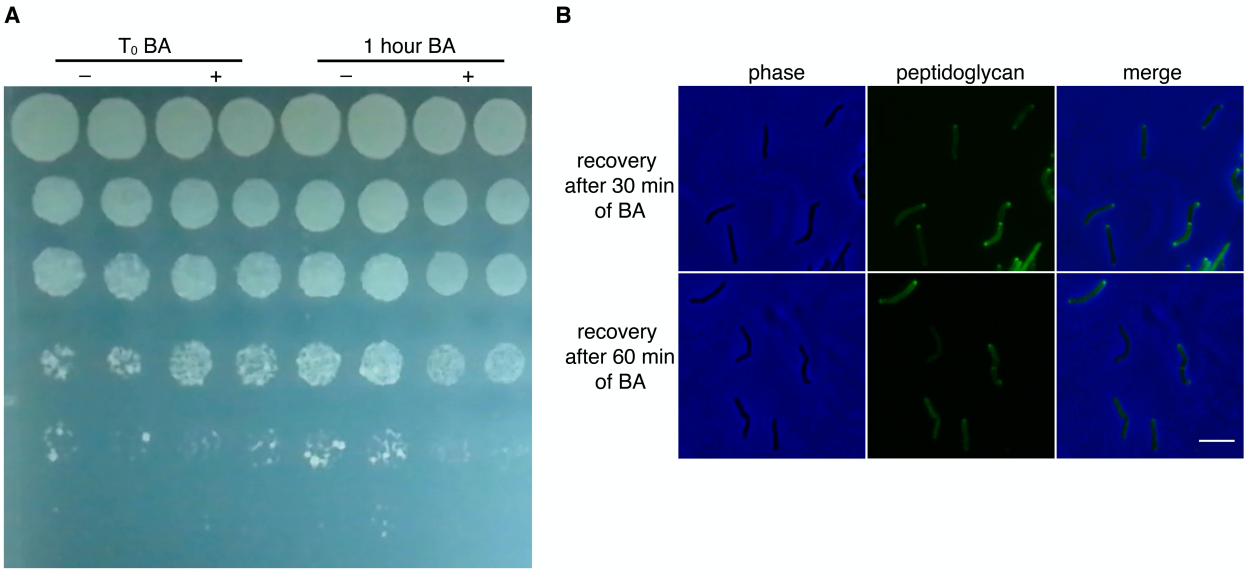

721

722 **Figure 3–figure supplement 3.** *M. smegmatis* survives benzyl alcohol (BA) treatment. (A) *M.*
723 *smegmatis* was treated with benzyl alcohol then washed in PBS. Ten-fold serial dilutions were
724 spotted on LB agar. Shown are cells immediately after addition of benzyl alcohol (T_0) and after 1
725 hour of exposure. (B) *M. smegmatis* were treated with benzyl alcohol for 30 or 60 min, washed
726 and incubated for 2 hours in fresh 7H9. Cells were then labeled with alkDADA for 15 min and
727 then fixed and alkynes were detected by CuAAC to reveal active peptidoglycan metabolism.
728 Scale bar 5 µm.

729

730

731

732

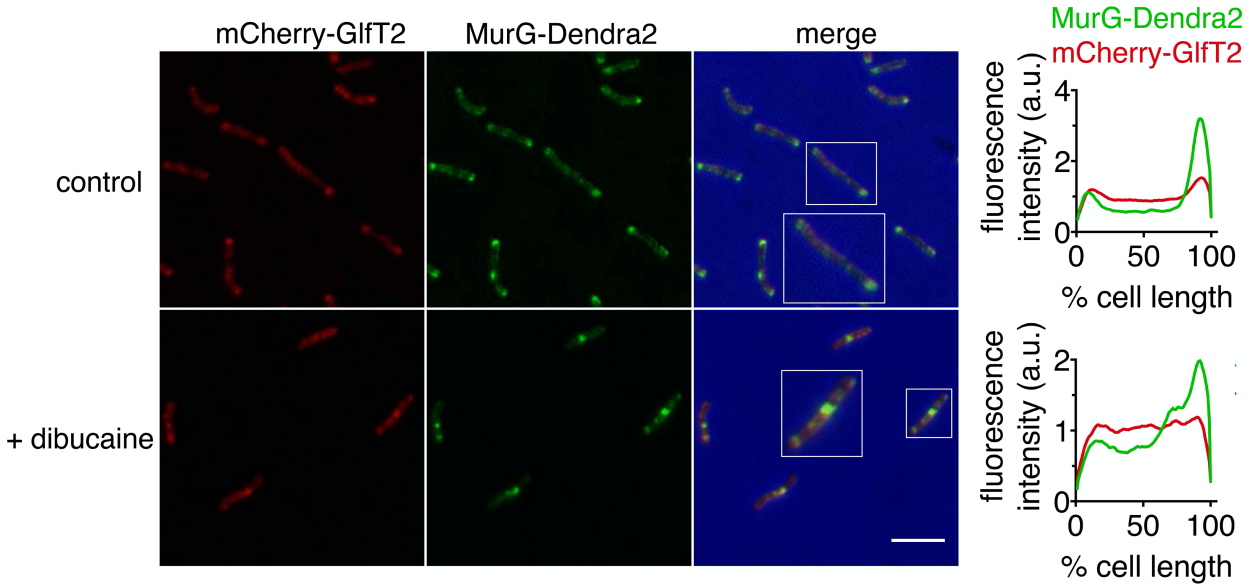

Figure 3–figure supplement 4. Dibucaine impacts the localization of MurG and GlfT2. *M. smegmatis* coexpressing the IMD-associated MurG-Dendra2 and mCherry-GlfT2 was treated or not with dibucaine. Images from conventional microscopy show these proteins lose their polar enrichment when treated with dibucaine. Scale bar, 5 μm. Right, the fluorescence intensity profiles of the fusion proteins were determined as in Figure 2A.

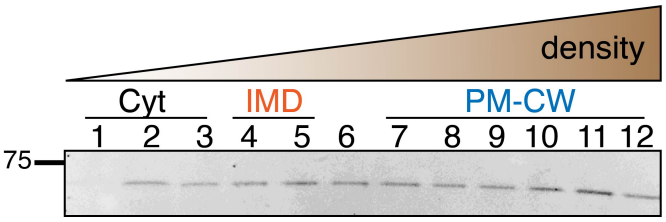

Figure 4–figure supplement 1. Cell wall is required for partitioning of MurG. *M. smegmatis* expressing MurG-Dendra2 were spheroplasted as in Fig. 4A and then lysed by nitrogen cavitation. The crude lysates were separated in a density gradient and blotted in a polyacrylamide gel. MurG-Dendra2 distributes widely along the membrane fractions consistent with the broad distribution of cellular material across the density gradient (see Fig. 4A), which contrasts with its normal partitioning (see Fig. 1C).

772 **Supplementary information**

Table S1. Incubation conditions		
Bacterium	Antibiotic or compound	Incubation conditions
M. smegmatis	100 mM benzyl alcohol	60 min at 37ºC with shaking
	50 mM dibucaine	180 min at 37ºC with shaking
DivIVA-eGFP-ID	50 ng/mL ATC	8 h, 14 to 16 h
MurJ-ID		8h
B. subtilis	24 µg/mL kanamycin	10 min at 37°C with shaking
	50 µg/mL phosphomycin	
	50 mM benzyl alcohol	
C. crescentus	5 µg/mL kanamycin	30 min at 30°C with shaking
	50 µg/mL phosphomycin	
	50 mM benzyl alcohol	
E. coli	20 µg/mL A22	90 min at 37°C with shaking. Cultures were back-diluted after 40 min of incubation to an OD_{600} ~0.3-0.5 in prewarmed medium + A22 and incubated until completion of 90 min
	16 µg/mL kanamycin	30 min at 37ºC with shaking
	50 µg/mL phosphomycin	
	50 mM benzyl alcohol	
S. aureus and *L. lactis*	50µg/mL phosphomycin	30 min at 37ºC with shaking
	20 µg/mL kanamycin	
	50 mM benzyl alcohol	
	50 µg/mL ampicillin (with 5 µg/mL clavulanate)	

773
774
775
776
777
778
779
780
781
782
783
784
785

Table S2. Incubation conditions of probes to metabolically label the cell envelope

Bacterium	Probe	Labeling conditions
M. smegmatis	alkDADA N-Alk-TMM O-Alk-TMM	Unless otherwise indicated, 15 min with shacking at 37ºC
E. coli *B. subtilis* *S. aureus* *L. lactis*	alkDADA	Unless otherwise indicated, 5 min with shacking at 37ºC
C. crescentus		Unless otherwise indicated, 5 min with shacking at 30ºC

Table S3. NCBI Accession numbers from 16S rDNA

Bacterium	NCBI accession number
M. smegmatis	AB305022.1
B. subtilis	NR_112116.2
S. aureus	NR_118997.2
L. lactis	FJ348447.1
E. coli	NR_024570.1
C. crescentus	NR_037099.1

808

809 **Table S4. Key Resources**

Reagent type	Designation	Source or reference	Additional information
Strain (*M. smegmatis* mc^{2}155)	*M. smegmatis*	NC_008596 in GenBank	Wild-type *M. smegmatis*
Strain (*M. smegmatis*)	MurG-Dendra2	This study	The mutant was generated as described in supplementary material and methods.
Strain (*M. smegmatis*)	mCherry-GlfT2	(Hayashi et al., 2016)	See reference for details.
Strain (*M. smegmatis*)	PonA1-mRFP	(Kieser et al., 2015)	Obtained from Dr. Eric Rubin (Harvard SPH) and Dr. Hesper Rego (Yale Med)
Strain (*M. smegmatis*)	PimE-GFP	This study	The mutant was generated as described in supplementary material and methods.
Strain (*M. smegmatis*)	MurG-ID depletion strain	(Meniche et al., 2014)	Obtained from Dr. Chris Sassetti (U Mass Med)
Strain (*M. smegmatis*)	MurJ-ID (MviN) depletion strain	(Gee et al., 2012)	Obtained from Dr. Chris Sassetti (U Mass Med)
Strain (*M. smegmatis*)	p_{tet}*ponA1*	(Hett et al., 2010)	Obtained from Dr. Eric Rubin (Harvard SPH)
Strain (*M. smegmatis*)	DivIVA-eGFP-ID	(Meniche et al., 2014)	Obtained from Dr. Chris Sassetti (U Mass Med)
Strain (*M. smegmatis*)	mCherry-GlfT2/DivIVA-eGFP-ID	This study	
Strain (*B. subtilis* JH642)	*B. subtilis*	NZ_CP007800 in GeneBank	
Strain (*C. crescentus*)	*C. crescentus*	NA 1000	Obtained from Dr. Peter Chien (U Mass Amherst)
Strain (*E. coli* K12)	*E. coli K12*	MG1655	
Strain (*S. aureus*)	*S. aureus*	ATCC BA-1718	Obtained from Dr. Thai Thayumanavan (U Mass Amherst)
Strain (*L. lactis*)	*L. lactis lactis*	NRRL B633	
Chemical compound	alkyne-D-alanine-D-alanine (alkDADA or EDA-DA)	(Liechti et al., 2014)	Synthesized by the Chemical Synthesis Core Facility at Albert Einstein College of Medicine (NY, USA) following the referenced protocols
Chemical compound	O-alkyne-trehalose monomycolate (O-AlkTMM)	(Foley et al., 2016)	Obtained from Dr. Benjamin Swarts (Central Michigan University)

Chemical compound	N-alkyne-trehalose monomycolate (N-AlkTMM)	(Foley et al., 2016)	Obtained from Dr. Benjamin Swarts (Central Michigan University)
Software, algorithm	MATLAB codes	(García-Heredia et al., 2018)	Scripts designed for MATLAB to analyze the fluorescence profiles along a cell body from data collected in Oufti[28].
Chemical compound	Fmoc-D-Lys(biotinyl)-OH BDL precursor	Chem-Impex International (Wood Dale, Il USA)	Deprotected as described in[13] to yield BDL
Chemical compound	A22 (S-3,4-Dichlorobenzylisothiourea hydrochloride)	Sigma-Aldrich, St. Louis, MO USA	Dissolved in water and kept at -20ºC
Recombinant DNA reagent	PBP4 plasmid	(Qiao et al., 2014)	Obtained from Dr. Suzanne Walker (Harvard Med)

810

811

812

813

814

815